Proceedings of the 3rd
RSI International Conference on Robotics and Mechatronics
October 7-9, 2015, Tehran, Iran

Effect of Structural Design Parameters of a Six-Axis Force/Torque Sensor Using Full Factorial Design

Amin Valizadeh, Alireza Akbarzadeh, Mohammad Hosein Tashakori Heravi
Center of Excellence on Soft Computing and Intelligent Information Processing (SCIIP)
Mechanical Engineering Department
Ferdowsi University of Mashhad
Mashhad, Iran
amin.valizadeh.66@gmail.com, ali_akbarzadeh_t@yahoo.com, mohamad.tashakori@gmail.com

***Abstract*—Force and torque sensors' various applicabilities have raised great interest among scientists for decades. The optimal combination of design variables is a difficult task as it is affected by several input parameters. This paper presents an investigation on the effect of thickness, width and length of elastic cross-beams of the six-axis force sensor on the cross coupling interference. The finite element analysis is carried out for full factorial design experiments and the signal to noise ratio as well as analysis of variance is calculated and discussed.**

Keywords—force and torque sensor; cross beams, full factorial design; signal to noise ratio; analysis of variance

I. INTRODUCTION

. The cross-beams force and torque sensors interests have been increased due to their benefits over the years. Various types of cross-beams force sensors were considered and developed in the 1980s [1, 2]. In the 1990s the field of studies mostly aims the industrial applications to perform a variety of tasks [3, 4]. Due to the expensive rate price of the six-axis F/T sensor, its application has been mainly confined to the robotics field, since precise force control is specifically essential for industrial manipulators. However, the development of economical cross-beams F/T sensors has strongly encouraged in various fields such as humanoid robots, biomechanics and medical applications [5, 6, 7]. Parallel and radial plates are extensively carried out as the main sensing elements of multi- component F/T sensors [8, 9]. Kim developed several multi- axis F/T sensors with an interference error of less than 3%, but they cannot be implemented on some applications for lack of proper size design [10, 11]. The United States and Japan have already advanced multiple multi-axis F/T sensors and they also lack affordable price [12, 13]. Cross-beams six-axis F/T sensors commonly categorized into two types according to the relationship between the applied force and the output signal: mechanically coupled sensors which the output signal must be calibrated with a relatively complicated calibration matrix, and mechanically decoupled sensors which the output signal of a bridge selectively responds to a specific force or moment component [14, 15]. In this paper, the cross coupling is conceptually defined as the ratio of unfavorable signal to the intended signal at a given bridge circuit according to pure force components. The cross coupling term yields the objective optimization equation which is carried out for different design parameters using full factorial design.

II. SIX-AXIS CROSS-BEAMS FORCE/TORQUE SENSOR

A. Mechanical Structure

A typical cross-beams six-axis force/torque sensor is illustrated in "Fig. 1". As it is shown, the model consists of six cross elastic beams which are symmetric horizontal beams (i.e., the section number 2), four compliant vertical beams (i.e., the section number 3) and a qubic center support (i.e., the section number 1). Where the vertical compliant beams connect the corresponding horizontal beams to the base (i.e., the section number 4), respectively. The whole model is manufactured monolithic and symmetric and hence all the parts have same material properties.

In the "Fig. 1", b, t, l are width, thickness and length of the horizontal elastic beams, and d and h are thickness and height of the vertical compliant beams, respectively. Typically we set the $b=t$, $d\leq 1/3\ b$ [16].

When the unknown load is applied to the force/torque sensor, the force and moment vectors can be considered a:

$$\vec{F} = F_x \hat{i} + F_y \hat{j} + F_z \hat{k} \tag{1}$$

$$\vec{M} = M_x \hat{i} + M_y \hat{j} + M_z \hat{k} \tag{2}$$

Where, Fx and Mx, Fy and My, Fz and Mz are the force and moment applied along the x, y and z direction to the qubic center support, respectively.

978-1-4673-7234-3/15/$31.00 ©2015 IEEE

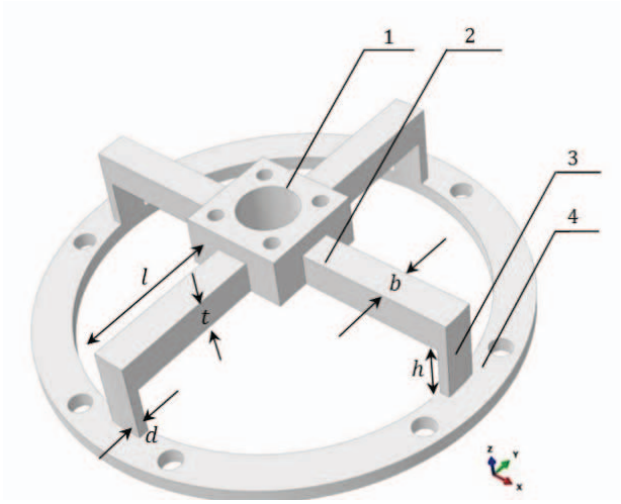

Fig. 1. Mechanical structure of a cross-beams six-axis force/torque sensor

B. Strain Gauges

In the six-axis force/torque sensor, 24 linear strain gauges required to measure the applied forces and torques in all three directions since with the smaller number of strain gauges, the sensor lacks the force measuring ability in some directions. The distribution of the 24 strain gauges is shown in "Fig. 2". According to the "Fig. 2", all the sensors measure axial strain where positive ones are tensile strains and the negative ones are compressive strains. Using the theory of "Mechanics of Material" six Wheatsone bridge circuits composed of four strain gauges are used in this study. "Table 1" specifies the strain gauges distribution for each bridge as well as the load components. The output strain of each load component is calculated using "(3)".

Consider a certain load applied to the six-axis sensor with the $F = [Fx\ Fy\ Fz\ Mx\ My\ Mz]^T$ components. The relationship between the load vector and the strain output vector in a 6 Wheatsone bridge circuits configuration, can be expressed by "(4)". Where [C] is a 6×6 strain compliance whose element C_{ij} represents the strain contribution at bridge circuit i due to a unit pure load j.

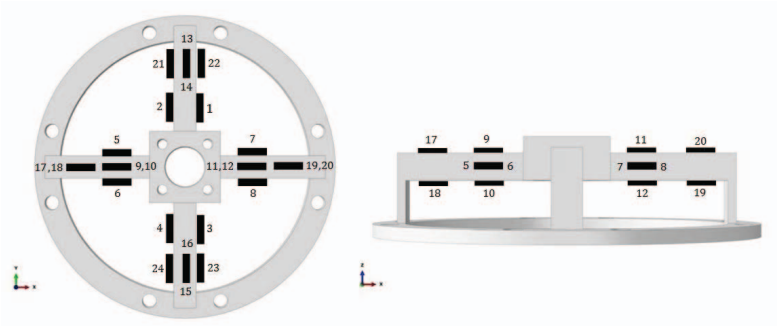

Fig. 2. Strain gauges disrtirbution of the six-axis force/torque sensor

TABLE I. WHEATSONE BRIDGE'S STRAIN GAUGES DISTRIBUTION

Load Componetnt	6-axis Force/Torque Sensor		
	Bridge Circuit No.	*Strain Gauges Distribution*	*Axis of measurment*
Fx	1	S_1, S_2, S_3, S_4	*y*-axis
Fy	2	S_5, S_6, S_7, S_8	*x*-axis
Fz	3	$S_9, S_{10}, S_{11}, S_{12}$	*x*-axis
Mx	4	$S_{13}, S_{14}, S_{15}, S_{16}$	*y*-axis
My	5	$S_{17}, S_{18}, S_{19}, S_{20}$	*x*-axis
Mz	6	$S_{21}, S_{22}, S_{23}, S_{24}$	*y*-axis

$$\begin{cases} S_{Fx} = \dfrac{S_1 - S_2 + S_3 - S_4}{4} \\ S_{Fy} = \dfrac{S_5 - S_6 + S_7 - S_8}{4} \\ S_{Fz} = \dfrac{S_9 - S_{10} + S_{11} - S_{12}}{4} \\ S_{Mx} = \dfrac{S_{13} - S_{14} + S_{15} - S_{16}}{4} \\ S_{My} = \dfrac{S_{17} - S_{18} + S_{19} - S_{20}}{4} \\ S_{Mz} = \dfrac{S_{21} - S_{22} + S_{23} - S_{24}}{4} \end{cases} \tag{3}$$

$$\vec{S}_{6\times1} = [C]_{6\times6} \times \vec{F}_{6\times1} \tag{4}$$

Under the 6 maximum pure load components as $\vec{F}_{\max} = [F_x^{\max} \quad F_y^{\max} \quad F_z^{\max} \quad M_x^{\max} \quad M_y^{\max} \quad M_z^{\max}]^T$, the strain matrix, S, can be defined by combining six C_j column vectors by "(5)".

The matrix in "(5)" is the leading factor for the definitions of cross coupling and principal coupling in the sensor.

$$S = [S_{ij}] = \begin{bmatrix} S_{11} & S_{12} & S_{13} & S_{14} & S_{15} & S_{16} \\ S_{21} & S_{22} & S_{23} & S_{24} & S_{25} & S_{26} \\ S_{31} & S_{32} & S_{33} & S_{34} & S_{35} & S_{36} \\ S_{41} & S_{42} & S_{43} & S_{44} & S_{45} & S_{46} \\ S_{51} & S_{52} & S_{53} & S_{54} & S_{55} & S_{56} \\ S_{61} & S_{62} & S_{63} & S_{64} & S_{65} & S_{66} \end{bmatrix} \tag{5}$$

Herein the cross coupling error $(CC)_{ij}$ is defined as:

$$(CC)_{ij} = \frac{S_{ij}}{S_{ii}} \tag{6}$$

where i = 1,..., 6 and $i \neq j$. Physically $(CC)_{ij}$ indicates the ratio of two output strains at bridge circuit i when maximum loads i and j are applied independently. In the design of a mechanically decoupled F/T sensor, the relative strain ratio $(CC)_{ii}$ should be minimized rather than unwanted strain S_{ij}, as the larger cross coupling error causes a decrease of resolution [17]. The cross-beams type sensors usually show larger $(CC)_{15}$ and $(CC)_{24}$ compared to other negligible $(CC)_{ij}$ values [11, 18]. Hence, we defined them as principal couplings which are as follows:

$$(CC)_{15} = \frac{S_{15}}{S_{11}} = \frac{M_y^{\max} C_{15}}{F_x^{\max} C_{11}}, (CC)_{24} = \frac{S_{24}}{S_{22}} = \frac{M_x^{\max} C_{24}}{F_y^{\max} C_{22}} \tag{7}$$

In "(7)", The coupling term $(CC)_{15}$ expresses the ratio of two strains under pure maximum moment My and pure maximum force Fx at the first bridge circuit, while $(CC)_{24}$ indicates the ratio of two strains under pure maximum moment Mx and pure maximum force Fy at the second bridge circuit. In this study, $(CC)_{15}$ and $(CC)_{24}$ are considered as principal coupling terms and the design optimization problem is formulated to minimize them. According to all the mechanical structure variables, the structural design optimization problem is considered as find [b, t, l] to minimize:

$$J(x) = \frac{\left|(CC)_{15}\right| + \left|(CC)_{24}\right|}{2} \tag{6}$$

The maximum von Mises stress to examine the exceeding of the material yield stress, the upper and lower bounds of strain outputs and the bandwidth applied load components should be noticed before taking "(8)" into action.

III. Finite Element Modeling

In order to evaluate the above properties, a finite element model in a commercial FEM software, ABAQUS, is designed. As "Fig. 3" depicts, the FEA model is designed by meshing all the regions into finite number of nodal elements with the size of 0.5 mm for each node. The model is constrained to be fixed at the ring shape base which are its static boundary conditions, and the load component is applied at the center of the qubic support center along the neutral axis of the elastic horizontal cross-beams. The Material used in this study is Aluminium (AL7075-T6) with the Young's modulus of 72×10^9 (Pa) and the Poissom ratio 0.33.

The variables to design the FEA model of F/T sensor are determined as follows:

- The rated capacity of the forces Fx, Fy and Fz is 20 N.
- The rated capacity of the moments Mx, My and Mz is 0.09 N.m.
- The attaching locations for each sensor in 6-axis force/moment was determined in consideration of the results of FEM analysis where the attachment location is 3mm and 6 mm from the center support. These locations are optimally gained by the FEM analysis results.

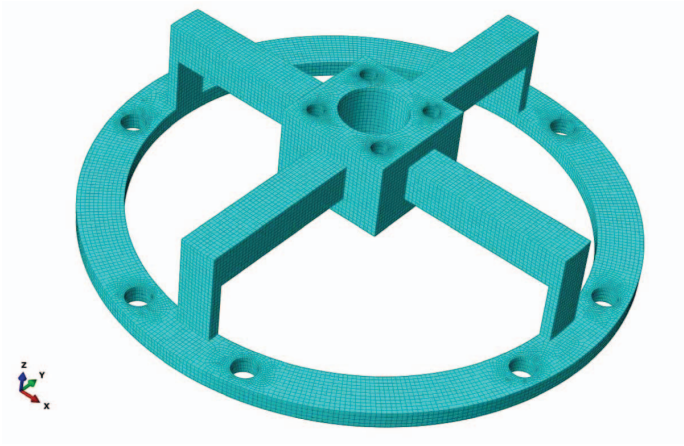

Fig. 3. The FEM model of the six-axis force/torque sensor

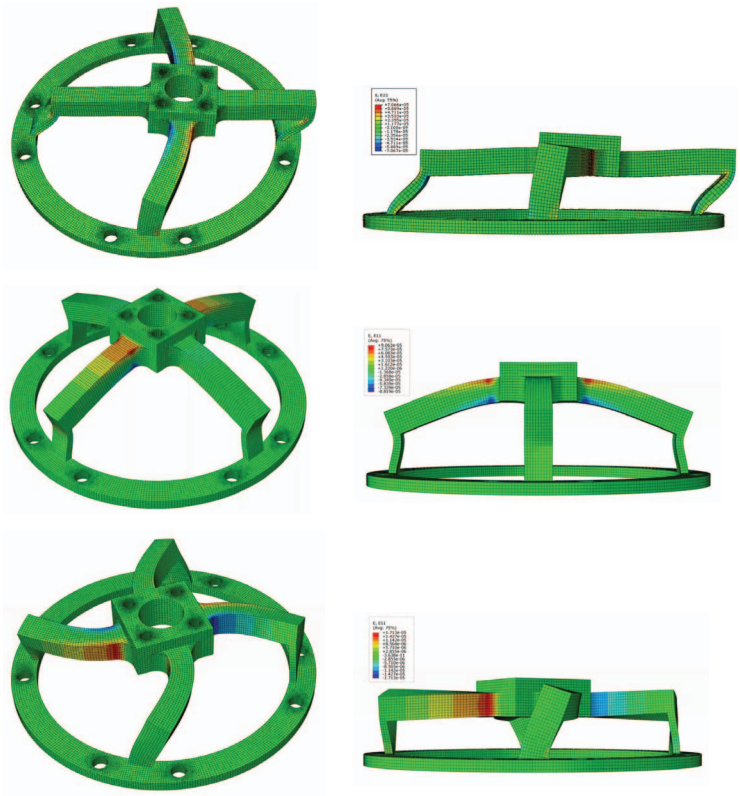

Fig. 4. Deformation of the FEM model under each single force/torque: I) Fx=20N II) Fz=20N III) Mz=0.09 N.m

TABLE II. THE STRAIN OUTPUTS UNDER EACH PURE MAX LOAD

Strain (μm/m)	Max Pure Load: F_x= F_y= F_z= 20 N M_x= M_y= M_z= 0.09 N.m Design Parameters: b= t =3 mm, l =21 mm					
	F_x	F_y	F_z	M_x	M_y	M_z
S_1	-76.3	-24.6	39.3	14.2	-11.8	-37.8
S_2	-76.4	-25	40	14.4	11.7	37.8
S_3	76.3	25.1	39.7	-14.4	-11.9	37.9
S_4	-76.4	24.7	39.6	-14.3	11.8	-37.9
S_5	25.1	76.2	39.7	11.9	14.4	-37.9
S_6	24.8	-76.4	39.6	-11.8	14.3	37.9
S_7	-24.8	76.3	39.3	11.8	-14.2	37.9
S_8	-25	-76.4	40	-11.7	-14.4	-37.9
S_9	72.9	15.2	16.8	2.3	68.8	-7.77
S_{10}	-47.1	15.8	-15.4	2.3	-67.9	-7.65
S_{11}	-72.2	-15.9	16.8	-2.3	-68.6	-7.78
S_{12}	46.5	15.9	-15.4	2.3	67.7	7.79
S_{13}	12	-43.5	12.7	55.3	-2.2	-6.14
S_{14}	-12	17.6	-11.3	-54.3	2.2	6.14
S_{15}	-12	-18.2	-11.3	54.5	2.1	-6.27
S_{16}	-12	43.5	12.7	-55.5	2.2	-6.18
S_{17}	43.6	12.1	12.7	1.8	55.5	-6.29
S_{18}	-18.1	12.5	-11.3	1.8	-54.5	-6.19
S_{19}	17.7	12.6	-11.3	1.8	54.4	6.29
S_{20}	-43.1	-12.6	12.7	-1.8	-54.4	-6.3
S_{21}	-61	-18.8	31.4	11.6	9.38	30.7
S_{22}	61	-18.5	30.8	11.4	-9.42	-30.7
S_{23}	61	19	31.1	-11.6	-9.5	30.7
S_{24}	-61	18.7	31	-11.6	9.5	-30.7

The deformations of the F/T sensor under each single maxload calculated by the FEM software are shown in "Fig. 4", and the strain outputs are seen in the "Table II". Substituting the strain outputs in "Table II" into "(3)" and "(4)" yields the strain output matrix by "(9)" which is significant for next steps

$$S_y = \begin{bmatrix} 0.0038 & 0.0000 & 0.0000 & -0.0008 & -0.1311 & 0.0006 \\ 0.0000 & 0.0038 & 0.0000 & 0.1311 & 0.0008 & -0.0006 \\ 0.0000 & -0.0004 & 0.0081 & -0.0122 & 0.0011 & -0.0436 \\ 0.0003 & -0.0015 & 0.0000 & 0.6100 & -0.0107 & -0.0343 \\ 0.0015 & 0.0003 & 0.0000 & 0.0103 & 0.6108 & 0.0347 \\ 0.0000 & 0.0000 & 0.0000 & 0.0006 & -0.0004 & 0.3417 \end{bmatrix} \times 10^{-3} \quad (9)$$

IV. RESULTS AND DISCUSSION

Full factorial design at 2-levels and 3-levels are the most frequently methods used in manufacturing experimental designs. Full factorial designed experiment consists of all possible combinations of levels for all factors. The total number of experiments for studying k factors at 2-levels is 2^k. The 2^k full factorial design is particularly appropriate in our study since this method is significantly useful when the number of design parameters is less than or equal to 4. According to the structural design optimization problem discussed, 8 tests were performed based on "Table III".

TABLE III. RESULTS OF EXPERIMENTS FOR THE OBJECTIVE OPTIMIZATION FUNCTION REGARD TO FULL FACTORIAL DESIGN

Test No.	Full Factorial Design Parameters			Optimization Function $J(x)$
	b (mm)	t (mm)	l (mm)	
1	3	3	19	0.30%
2	3	3	21	0.34%
3	4.5	3	19	0.29%
4	4.5	3	21	0.33%
5	3	4.5	19	0.14%
6	3	4.5	21	0.16%
7	4.5	4.5	19	0.15%
8	4.5	4.5	21	0.17%

A. Signal to Noise Ratio & Analysis of Variance

The S/N ratio is the ratio of signal to noise which signal and noise represent the desirable (i.e., the mean for the output characteristics) and undesirable value (i.e., the squared deviations for output characteristics), respectively. S/N ratio is used to evaluate the quality characteristics of the experimentally observed values which the three general categories are the larger of better, the smaller the better and nominal is better [19]. The characteristic considered is the optimization function hence the lower value represents the lower cross coupling error, that is to say "smaller is better". The S/N ratio can be expressed as a logarithmic transformation of the loss function using "(10)" and is shown in "Table IV".

$$S/N = -10\log\frac{1}{n}\sum_{i=1}^{n} y^2 \quad (10)$$

TABLE IV. S/N RATIO FOR OPTIMIZATION FUNCTION

Level	b	t	l
1	0.2350	0.3150	0.2200
2	0.2350	0.1550	0.2500
Delta	0.0000	0.1600	0.0300
Rank	3	1	2

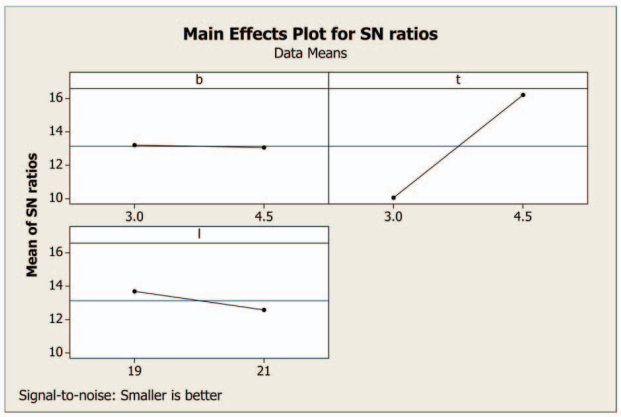

Fig. 5. Plot of S/N ratio fot the optimization function of six-axis F/T sensor

From the S/N ration as shown in "Table IV", it is observed that the optimal parameter combination for minimizing the cross coupling error, is at beam thickness (t) level 2 and beam length (l) level 1. In other words, increasing the thickness of the beam likewise decreasing the length of it causes the beam to bend and hence the better strain output results. Also, the negligible effect of beam width (b) on cross coupling error is clear from the results.

Finally, a statistical analysis of variance (ANOVA) is performed to see which design parameters are statistically significant. The level of importance of the variable parameters on the cross coupling error has been determined by using analysis of variance as illustrated in "Table V".

TABLE V. PERCENTAGE OF IMPORTANCE OF THE DESIGN PARAMETERS USING ANOVA

Factors	***b***	***t***	***l***
%	≤1	96.3	3.1

"Table V" expresses the importance of elastic cross-beams thickness is far more than two other parameters, while the width of the cross-beams has inconsiderable effect on cross coupling error. As a result, the model in test number 5 from "Table II" has the best design parameter combination due to minimize the cross coupling error.

V. CONCLUSION

The effect of the structural design parameters on decreasingthe cross coupling interference for a six-axis force/torque sensor was investigated. Thickness, width and length of the elastic cross-beams are the design parameters which are considered in this study. A 2-level full factorial approach was carried out and 8 tests were experimented in a commercial finite element software, ABAQUS. The statistical analysis of results shows that the thickness of the cross-beams has the most remarkable effect on minimizing the cross coupling error.

REFERENCES

[1] G. Piller, "A compact six degree fo freedom force sensor for assembly robot," 12th International Symposium on Industrial Robots, Paris, France, pp. 121-129, June 1982.

[2] Zy. Nakamuro, T. Yoshikawa, Futamata, "Design and singal processing of six-axis force sensor," 4th International Symposium of Robotics Research, Cambridge, MA, USA, pp. 75-81, 1987.

[3] M. Perry, "Multi-axis force and torque sensing," Sensor Rev., vol. 17, 1997, pp. 117-120.

[4] Y.F. Li, X.B. Chen, "On the dynamic behavior of a force/ torque sensor for robots," IEEE Trans. Instrum. Means., vol. 47, pp. 304-308, February 1998.

[5] T. Liu, Y. Inoue, K. Shibata, "Wearable force sensor with parallel structure for measurement of ground-reaction force," Measurement, vol. 40, 2007, pp. 644-653.

[6] J.H. Kim, J.H. Oh, "Realization of dynamic walking for the humanoid robot platform KHR-1," Adv. Robot., vol. 18, 2004, pp. 749-768.

[7] J.H. Kim, J.W. Han, D.Y. Kim, Y.S. Baek, "Design of a walking assistance lower limb exoskeleton for paraplegic patients and hardware validation using CoP," Adv. Robot. Syst., vol. 10, 2013, pp. 11-13.

[8] Y. Hatamura, K. Matsumoto, H. A. Morishita, "A miniature 6-axis force sensor of multi-layer parallel plate structure," IMEKO, 1989, pp. 567-82.

[9] K. Ono, Y. Hatamura, "A new design for 6-component force/torque sensors," Mecahnical Problems in Measuring Force and Mass, H. Wieringa, Ed., Martinus Nijhoff, Dordecht, 1986, pp. 39-48.

[10] G. S. Kim, D. I. Kang, S. H. Rhee, K. W. Um, "Design and fabrication of a 3-component force/moment sensor using the plate-beams," Meas. Sci. Technol., vol. 10, 1999, pp. 295-301.

[11] G.S. Kim, "Design of a six-axis wrist force/moment sensor using FEM and its fabrication for an intelligent robot," Sensor Actuat. A-Phys., vol. 133, 2007, pp. 27-34.

[12] ATI Industrial Automation, "Multi-Axis Forcr/Torque Sensor," ATI Industrial Automation, 2005, pp. 4-45.

[13] Nisso Electric Works Co., Ltd, "Multi Component Loadcell," Nisso Electric Works Co., Ltd, 1999, pp. 5-32.

[14] L.P. Chao, K.T. Chen, "Shape optimal design and force sensitivity evaluation of six-axis force sensors," Sensor Actuat. A-Phys., vol. 63, 1997, pp. 105-112.

[15] S. A. Liu, H.L., Tzo, "A novel six-component force sensor of good measurement isotropy and sensitivities," Sensor Actuat. A-Phys., vol. 100, 2002, pp. 223-230.

[16] Song A., Wu J., Qin G., Huang W., "A novel self-decoupled four degree-of-freedom wrist force/torque sensor," Measurement, vol. 40, 2007, pp. 883-891.

[17] M.K. Kang, S. Lee and J. H. Kim, "Shape Optimization of a Mechanically Decoupled Six-Axis Force/Torque Sensor," Sensors Actuat. A-Phys., vol. 209, 2014, pp. 41-51.

[18] L.P. Chao, K.T. Chen, "Shape optimal design and force sensitivity evaluation of six-axis force sensors," Sensor Actuat. A-Phys., vol. 63, 1997, pp. 105-112.

[19] Yan-Cherng Lin, Han-Ming Chow, Biing-Hwa Yan, Hsinn-Jyh Tzeng, "Effects of finishing in abrasive fluid machining on microholes fabricated by EDM" Adv. Manuf. Technology, vol. 33, 2007, pp. 489-497.